This manuscript was accepted by Rev. Sci.Instrum. Click here to see the version of record.

Combined scanning probe microscopy and X-ray scattering instrument for in situ catalysis investigations

Willem G. Onderwaater,[1,2] Peter C. van der Tuijn,[1,3] Rik V. Mom,[1] Matthijs A. van Spronsen,[1,4] Sander B. Roobol,[1,5] Amirmehdi Saedi,[1] Jakub Drnec,[2] Helena Isern,[2] Francesco Carla,[2] Thomas Dufrane,[2] Raymond Koehler,[1] Bert Crama,[1] I. M. N. Groot,[6,1,a)] Roberto Felici,[2] and J. W. M. Frenken[1,7]

[1)] *Huygens-Kamerlingh Onnes Laboratory, Leiden University, P.O. Box 9504, 2300 RA Leiden, the Netherlands*

[2)] *European Synchrotron Radiation Facility, BP 220, F-38043 Grenoble Cedex 9, France*

[3)] *Current address: Leiden Probe Microscopy B.V., J.H. Oortweg 19, 2333 CH Leiden, the Netherlands*

[4)] *Current address: Department of Chemistry and Chemical Biology, Harvard University, Cambridge, Massachusetts 02138, United States*

[5)] *Current address: ASML Netherlands B.V., De Run 6501, 5504 DR Veldhoven, the Netherlands*

[6)] *Gorlaeus Laboratories, Leiden University, P.O. Box 9502, 2300 RA Leiden, the Netherlands*

[7)] *Current address: Advanced Research Center for Nanolithography, P.O. Box 93019, 1090 BA Amsterdam, the Netherlands*

(Dated: 7 November 2016)

We have developed a new instrument combining a scanning probe microscope (SPM) and an X-ray scattering platform for ambient-pressure catalysis studies. The two instruments are integrated with a flow reactor and an ultra-high vacuum system that can be mounted easily on the diffractometer at a synchrotron end station. This makes it possible to perform SPM and X-ray scattering experiments in the same instrument under identical conditions that are relevant for catalysis.

[a)] Electronic mail: i.m.n.groot@lic.leidenuniv.nl

This manuscript was accepted by Rev. Sci.Instrum. Click here to see the version of record.

I. INTRODUCTION

In recent years, operando catalysis research has witnessed the development of a number of experimental surface-science techniques for application under harsh conditions, approaching those of industrial catalysis. Examples are X-ray photoelectron spectroscopy (XPS)[1], X-ray scattering techniques[2,3], transmission electron microscopy (TEM)[4,5], scanning tunneling microscopy (STM)[6–8], and atomic force microscopy (AFM)[9], which have been developed to investigate a wide array of relevant catalytic systems, ranging from single-crystal model catalysts to supported nanoparticles. Each of these techniques contributes only a specific component to our understanding of heterogeneous catalysis. In view of the complexity of catalytic processes, techniques have to be combined in order to arrive at a sufficiently complete description of the working mechanisms of a catalyst. Unfortunately, combining information from different techniques is not straightforward since a catalyst under operating conditions is a dynamical system that depends on numerous other factors, such as reactor geometry, sample size, gas flow rates, etc. Every technique introduces constraints that often make it difficult to study catalysts in precisely the same environment.

This paper describes the integration of a scanning probe microscope (SPM) with an X-ray scattering platform in a gas flow reactor combined with an ultra-high vacuum (UHV) system that can be mounted on a diffractometer. With this experimental set-up we can directly combine X-ray scattering data with real-space information obtained with the microscope. Independently, both X-ray techniques and SPM have proven to be powerful tools for understanding surface structures in operando conditions[10–13]. Nonetheless, both techniques possess a number of limitations that can be circumvented by combining the two techniques in one instrument.

One of the limitations of the generally employed X-ray techniques such as surface X-ray diffraction (SXRD) and grazing incidence small angle X-Ray scattering (GISAXS) is that these are averaging techniques, i.e. they rely on the addition, coherent or incoherent, of photons originating from a large volume of scatterers[14,15]. For in situ catalysis experiments this volume consists of a collection of nanoparticles or a large single-crystal surface area. In the interpretation of these averaging experiments, the assumption is usually made that the entire area illuminated by X-rays exhibits the same characteristics. This assumption, however, is not always justified. In the case of nanoparticles, signal averaging results in a

convolution of the signals originating from the individual particles. These are impossible to disentangle without additional information. A frequently employed work-around for this limitation is to analyze the nanoparticle ensemble before and after the catalysis experiment with a measurement technique such as scanning electron microscopy (SEM). This way, the size distribution of the nanoparticles can be measured accurately. However, because the distribution changes during the catalytic activity of the nanoparticles, the connection between the X-ray data and the particle distribution can be still difficult to make.

In contrast, because STM and AFM only probe a small area of the catalyst, these results do not suffer from averaging effects. But, as mentioned before, there is no guarantee that the imaged area is representative of the entire surface. A second limitation of SPM is that it only probes the top atomic layer, while interesting phenomena might be occurring below. Finally, even though STM and AFM images display clear, atomic-scale features, it is challenging to extract quantitative structural information directly from the images.

The limitations of the two classes of techniques, real space and reciprocal space, can be largely overcome by combining them in a single instrument. For example, for a catalyst composed of nanoparticles the combination will make it straightforward to obtain information about their size distribution, spatial ordering, and internal structure. By gathering the SPM and X-ray data in the same set-up under the same experimental conditions, one can be certain that they reflect precisely the same state of the model catalyst.

The use of SPM techniques at synchrotron beamlines is well established. AFM and STM are used in combination with synchrotron radiation for combined imaging and spectroscopy[16–25]. The SPM-X-ray combination presented here, integrated with a UHV chamber and a gas flow reactor, enables the application of this combination of techniques to the field of heterogeneous catalysis.

In this paper, we describe the design and performance of the combined SPM and X-ray scattering instrument. A complete view of the set-up is presented in Figure 1. Our design is based on the ReactorSXRD setup[26] that has been developed previously at the ID03 beamline of the European Synchrotron Radiation Facility (ESRF) for in situ study of catalyst surfaces by surface X-ray diffraction[27] and on the ReactorSTM[7] and ReactorAFM[9] set-ups that have been developed earlier at Leiden University. It combines a UHV system for sample preparation procedures with a flow reactor in which gas pressures up to 1 bar and sample temperatures up to 1000 °C can be achieved. The SPM part of the new instrument

is integrated with the flow reactor. This enables us to image catalytically active systems in situ, in real space with the SPM, and in reciprocal space using the X-rays.

II. DESIGN

As the basis for our design, we have used the ReactorSXRD set-up that has been developed previously for high-pressure, high-temperature SXRD experiments on model catalysts. This instrument satisfies all requirements for in situ X-ray scattering experiments[26]. Here, we first summarize the special features of this set-up and then discuss its combination with the SPM unit. For further details of the ReactorSXRD design and performance, we refer to Ref. 26.

In short, the ReactorSXRD instrument consists of a UHV chamber and a flow reactor. The UHV chamber is formed by a large-diameter bellow between two horizontal flanges. The bottom flange is connected to the diffractometer and contains a central pillar onto which the sample holder is mounted. Using a motor drive and a set of spindles, the top flange can be translated up and down in a controlled manner. In this way, one can choose for a geometry with the top flange in an upper position in which the sample is fully in the UHV environment, while an evaporation source and an ion gun are aligned with the surface; this configuration is used for sample preparation. With the top flange in the lower position, a seal structure between the sample support and the top flange makes a nearly UHV-tight separation between the reactor volume and the UHV chamber. In this configuration, the sample is surrounded by a hemispherical dome of an X-ray-transparent material. Gas tubes in the sample support column are used to supply the small 60 mL reactor volume with a flow of a gas mixture, of which we independently control the composition, the pressure, and the flow rate over relatively large ranges.

For X-ray scattering experiments, we use a beryllium dome, in view of its excellent transmission for X-rays. We have developed an alternative, dedicated aluminum dome for the combined X-ray and SPM experiments. A miniature SPM unit has been constructed that can operate in a chemically harsh, high-temperature, high-pressure environment. It is mounted on top of the aluminum dome.

The geometry of the combined instrument has been kept completely modular, which enables us to exchange components easily and switch between STM, AFM, or SXRD modes

of operation.

In the remainder of this section, we will provide a more detailed description of the part of the set-up that is shown in Figure 2, which contains the essential new elements, such as the aluminum dome and the SPM part.

A. X-ray-transparent dome

The dome is made by 3D printing of aluminum. The wall thickness is 1 mm, which results in a transmission coefficient of 0.6 at 24 keV. The dome thickness currently restricts the X-ray experiments to hard X-rays with energies above 18 keV. Construction of a thinner beryllium dome would allow one to also use lower-energy X-rays. The SPM part of the instrument is mounted on top of the dome and reaches in towards the sample surface along the central axis of the dome and the sample. The shape of the SPM part is kept as slender as possible so that scattered X-rays can reflect off the surface without being blocked by SPM components up to an angle of 40° with respect to the sample surface, and over a 130°-range of azimuthal angles. The dome serves as the reactor and has a volume of 60 mL. The SPM part that sticks into the dome reduces the effective reactor volume to 40 mL.

B. Mechanical design of the scanning probe microscope

The basic configuration of the SPM part of the system is the same as that of the ReactorSTM and the ReactorAFM that have been described in detail in Refs.[7,9]. Central to the design is a cylindrical piezo element that is used for the X-, Y-, and Z-motion. The same piezo element serves as the actuator of a stick-slip translation stage for the coarse approach of the tip or the quartz tuning fork with tip to the surface. This motion is performed by a compact slider that moves inside a polyetherimide (PEI) tube and is pulled against isolated contact rails embedded in the inner wall of that tube, by a CoSm magnet. In this way, the slider provides the required electrical connections to the tip or the tuning fork with tip. The system is configured such, that the piezo element is not in contact with the gas atmosphere inside the dome. Only the PEI tube with the slider and the tip or tuning fork with tip is exposed to the dome's atmosphere (see Figure 2). The piezo element and the wiring of the microscope remain in a separate housing that is evacuated prior to the experiment to

a moderate vacuum. Feedthroughs in the top of this housing connect the wiring of the microscope to external cables that are guided away in order not to block the in- or outgoing X-rays (indicated by red arrows in Figure 2).

The complete SPM unit including the aluminum dome has a height of 20 cm (see Figure 2). This compact SPM design naturally leads to high mechanical resonance frequencies, which is beneficial for making the instrument minimally sensitive to external vibrations. Switching between STM and AFM modes is straightforward, as it merely requires replacing the slider carrying the probe — either the tip or the quartz tuning fork with tip — and the electronics that connect to the probe.

The mechanical loop that determines the sensitivity of the microscope to external vibrations includes the sample, the sample holder, the holder's supporting structure, the top flange of the UHV chamber, the aluminum dome, the base plate on which the piezo tube is mounted, the piezo element itself, the aluminum tube, the slider and, finally, the tip or combination of tuning fork with tip. In order to eliminate all flexibility in this loop, the top flange of the UHV chamber has to be maximally lowered[26]. Unfortunately, this reduces the leak from the reactor volume to the UHV chamber effectively to zero, so that we cannot use the mass spectrometer on that chamber for gas analysis simultaneously with SPM imaging. We have solved this by attaching an additional UHV chamber with residual gas analyzer to the exhaust gas line of the reactor.

In order to isolate the microscope as much as possible from external, mechanical, and acoustical vibrations, the pumps connected to the reactor exhaust, the turbomolecular pump of the UHV chamber, and of the gas manifold are all placed outside the experimental hutch. The roughing pumps backing up the turbomolecular pump and pumping the gas flow from the reactor exhaust are connected with 10 m long, plastic bellows via a lead mass, separating most of the pump vibrations. The other pumps also have 10 m plastic bellows, but are directly connected to the gas manifold and the connector plate.

C. Control electronics

The microscope is controlled by SPM electronics from Leiden Probe Microscopy BV[28], which features a digitally controlled fast analog scan generator and a high-bandwidth analog feedback system for high-speed imaging. As a complicating factor, the feedback settings of

this system are controlled by several analog potentiometers, requiring direct access to the electronics. Therefore, it was necessary to place the entire SPM control system inside the control room, at a distance of 20 m from the microscope in the experimental hutch. One of the consequences of this large distance is the extra capacitance of 1 nF per electrode on the piezo element, introduced by the long cables to the high-voltage amplifiers. In STM mode, the bias voltage is applied to the sample via the thermocouple wires. We use a differential cable to bridge the 20 m to a separate amplifier, close to the diffractometer. This amplifier is designed to reject the common noise on the differential cable, which results in a low-noise bias voltage on the sample. The use of the thermocouple wires eliminates the possibility of measuring the temperature during imaging. This should not be a problem since we avoid changing temperature during STM or AFM imaging, as the sample would otherwise drift out of the range of the piezo element. In STM mode, we use a preamplifier close to the microscope to convert the tunneling current into a voltage. Again, differential cabling is used to connect this voltage over the 20 m to the SPM electronics in the control room. For the AFM mode, we use the same electrical read-out circuit as the ReactorAFM[9]. A Zurich Instruments HF2LI lock-in amplifier is placed in the experimental hutch, close to the microscope. It is connected to the LPM control system via four 20 m long BNC cables carrying the relevant signals from the force sensor.

III. PERFORMANCE

The modularity of this system works well. With the top flange of the UHV system in the lower position, the UHV side is sealed off from the reactor volume, which can be opened readily to change tips and samples or to change from STM to AFM mode or vice versa. This can be done on a timescale of minutes. Via the gas lines, the reactor volume can be pumped down to a moderate vacuum, prior to raising the top flange and connecting the reactor with the UHV chamber. The complete assembly fits well on the diffractometer and can be rotated easily around all diffractometer axes, without problematic situations arising from the connecting cables and capillaries. As will be demonstrated below, the X-ray scattering performance of the instrument is not compromised by the combination with the SPM part. As expected, the SPM resolution is modest but atomic steps are imaged routinely with the instrument. So far, we have only used the instrument in the STM mode. The performance

of the AFM will be the subject of future work.

The performance of the SPM scanner was tested in air at room temperature on a table top catalysis chamber. This chamber has the same type of sample holder and mechanical loop as the ReactorSXRD chamber, but it was supported by a vibration isolation system, so that it was only exposed to a low level of vibrational noise. Therefore, this configuration results in a better SPM performance compared to mounted in the ReactorSXRD chamber. Under these favorable conditions, the STM images of Au(111) showed clear step resolution and structures can be distinguished on the terraces (left-hand panel of Figure 3). The holes observed in the terraces are caused by the presence of sulfur on the surface. As the right-hand panel of Figure 3 shows, when the vibration isolation system is removed and the set-up is mounted on the diffractometer, the SPM images still exhibit step resolution. Some of the vibrational eigenmodes of the mechanical loop of the SPM, in particular the one at 370 Hz, provide a dominant contribution to the images. These mechanical resonances are excited mainly by the vibrations of the floor of the ESRF laboratory building.

The first full test of the system on the diffractometer under catalytic conditions was performed in STM mode with a PtIr tip using a Pd(100) surface. We cleaned the surface in the UHV chamber by repeated cycles of 1000 eV argon ion bombardment and annealing at 1150 K. After this we lowered the top flange to seal off the reactor volume from the UHV chamber. We then used four different techniques to inspect the sample, namely STM (Figure 4), X-Ray Reflectivity (XRR) (Figure 5), SXRD (Figure 5), and GISAXS (Figure 6). For the X-ray measurements the photon energy was set to 24 keV. We show measurements at three stages in the exposure of the Pd surface to different mixtures of CO and O_2, all at a total gas pressure of 1.1 bar and a sample temperature of 300 °C; (i) under initial, reducing conditions in a flow of 30 ml/min CO and 40 ml/min O_2, (ii) after oxidation of the surface in 3 ml/min CO and 55 ml/min O_2, and (iii) after subsequent reduction in 20 ml/min CO and 38 ml/min O_2.

In the initial mixture of CO and O_2 with flows of 30 ml/min CO and 40 ml/min O_2, the Pd(100) surface is flat as illustrated by the reflectivity curve and the crystal truncation rod (red curves) in both panels of Figure 5 (the intensity between the crystal truncation rods scales with smoothness). We proceeded by exposing the surface to a mixture of CO and O_2 with flows of 3 ml/min CO and 55 ml/min O_2. In this environment the surface became oxidized and developed significant roughness, as is illustrated by the STM image in the

left-hand panel of Figure 4. The two blue curves in Figure 5 show the presence of roughness by the steep decay of the intensity away from the Bragg peaks and the negligible intensity between the Bragg peaks[12,29,30]. A similar effect can be recognized in the GISAXS pattern in the left-hand panel of Figure 6 and the blue curve in the right-hand panel of Figure 6 (a wide pattern means a rough surface). The gas mixture was changed again, now with flows of 20 ml/min CO and 38 ml/min O_2. Under these conditions the STM image shows a different surface topography than in the previous conditions which we ascribe to a reduction of the surface. This was confirmed by the disappearance of the diffraction signal of the oxide (not shown). Both the reflectivity curve and the [1 0 l] rod recover their initial shape as can be seen in Figure 5. The GISAXS pattern for this gas mixture shows a smoothening of the surface as can be seen from the decrease in scattered intensity at high values of $q_{\|}$ in the right-hand panel of Figure 6. Summarizing, from the STM images shown in Figure 4b we see that the roughening of the surface is inhomogeneous. This is information one cannot obtain from X-ray data. However, the X-ray data supply more information on the average roughness, as cannot be obtained from a local surface probe as is STM.

In Figure 6, we show two GISAXS patterns of the Pd(100) surface. The right-hand panel in Figure 6 shows two cuts through these patterns with the intensity against parallel momentum transfer $q_{\|}$ at a fixed q_z value, corresponding to the Yoneda peak. For the reduced surface, with flows of 20 ml/min CO and 38 ml/min O_2, the intensity decays more slowly with $q_{\|}$. This can be interpreted as the result of the smoothening of the metallic surface[12,29,30], enabled by the increased surface mobility after the removal of the oxide[31].

Like most SPM instruments, our SPM is sensitive to thermal drift. To a large extent, this is due to the construction of the sample holder, which has not been designed to expand symmetrically and with a fixed height of the surface plane when the temperature is increased. The typical timescale for the system to reach steady imaging conditions with a drift rate below 50 nm/min, after a large, e.g. 100° C, change in sample temperature, is 3 hours. Changes in temperature distribution induced by gas-composition changes are within the thermal window of the microscope, provided that the heat capacity of the gas mixture does not change too much.

The time it takes to switch from X-ray measurements to SPM operation is mainly determined by the speed of the coarse approach mechanism of the tip. The approach can be time consuming since the initial distance between the sample and the tip apex is unknown,

ing that the entire approach trajectory has to be traversed in small, sub-micrometer steps. After each approach step, a sensing procedure is performed to establish whether the tip is already close enough to the surface. Alternatively, we can use the X-ray beam to accurately measure the distance between the tip and the sample, reducing the approach time from hours to minutes. After the SPM measurements have been completed, the slider can be retracted and X-ray measurements can recommence. Since the sample remains aligned during SPM measurements, no realignment has to be performed.

We have performed preliminary simultaneous STM and X-ray reflectivity measurements that have demonstrated that the combination of the two measurements is really possible at the same time. However, the photoelectrons generated by the incident X-rays provide a significant contribution to the current measured by the STM tip. When the X-ray beam intensity is increased, as is necessary for SXRD measurements, this current contribution becomes dominant with respect to the tunneling current and makes it difficult to use the measured current as the control signal for the STM imaging. This difficulty can be reduced greatly by replacing the STM tip by a tailor-made, coaxial tip configuration, in which most of the photoelectron current is captured by a separate outer electrode (shield). This forms a rather involved addition to the experimental set-up but it opens completely new experimental possibilities, which we have explored recently and will report in a future publication.

IV. CONCLUSION AND OUTLOOK

We have developed an instrument for combined synchrotron X-ray scattering and scanning probe experiments for in situ catalysis studies. This new instrument allows us to perform a real-space characterization of the surface topography and a determination of the surface structure under identical high-pressure, high-temperature catalytic conditions. Both scanning tunneling microscopy and atomic force microscopy can be performed. This instrument contributes to the understanding of fundamental reaction processes by making it possible to follow the evolution of the structure and morphology of active catalytic systems in response to the temperature and gas environment to which they are exposed.

We have constructed the instrument in a modular fashion, combining the previously developed ReactorSXRD system for synchrotron X-ray studies with the technology of our ReactorSTM and ReactorAFM systems previously developed for SPM studies under cat-

nlgtic conditions, in a very compact fashion. The "bolt-on" SPM unit developed here can be combined also with other reactor configurations, such as the table-top catalysis chamber, used in some of the SPM performance tests.

REFERENCES

[1]H. Bluhm, M. Hävecker, A. Knop-Gericke, M. Kiskinova, R. Schlögl, and M. Salmeron, MRS bulletin **32**, 1022 (2007).

[2]S. Ferrer, M. D. Ackermann, and E. Lundgren, MRS bulletin **32**, 1010 (2007).

[3]D. D. Fong, C. A. Lucas, M. I. Richard, and M. F. Toney, MRS bulletin **35**, 504 (2010).

[4]P. L. Gai, E. D. Boyes, S. Helveg, P. L. Hansen, S. Giorgio, and C. R. Henry, MRS bulletin **32**, 1044 (2007).

[5]J. F. Creemer, S. Helveg, G. H. Hoveling, S. Ullmann, A. M. Molenbroek, P. M. Sarro, and H. W. Zandbergen, Ultramicroscopy **108**, 993 (2008).

[6]J. Frenken and B. Hendriksen, MRS bulletin **32**, 1015 (2007).

[7]C. T. Herbschleb, P. C. van der Tuijn, S. B. Roobol, V. Navarro, J. W. Bakker, Q. Liu, D. Stoltz, M. E. Canas-Ventura, G. Verdoes, M. A. van Spronsen, M. Bergman, L. Crama, I. Taminiau, A. Ofitserov, G. J. C. van Baarle, and J. W. M. Frenken, Review of Scientific Instruments **85**, 083703 (2014).

[8]M. A. van Spronsen, G. J. C. van Baarle, C. T. Herbschleb, J. W. M. Frenken, and I. M. N. Groot, Catalysis Today **244**, 85 (2015).

[9]S. B. Roobol, M. E. Canas-Ventura, M. Bergman, M. A. van Spronsen, W. G. Onderwaater, P. C. van der Tuijn, R. Koehler, A. Ofitserov, G. J. C. van Baarle, and J. W. M. Frenken, Review of Scientific Instruments **86**, 033706 (2015).

[10]M. D. Ackermann, T. Pedersen, B. Hendriksen, O. Robach, S. Bobaru, I. Popa, C. Quiros, H. Kim, B. Hammer, S. Ferrer, and J. W. M. Frenken, Physical Review Letters **95** (2005).

[11]B. L. M. Hendriksen, S. C. Bobaru, and J. W. M. Frenken, Surface Science **552**, 229 (2004).

[12]B. L. M. Hendriksen, M. D. Ackermann, R. van Rijn, D. Stoltz, I. Popa, O. Balmes, A. Resta, D. Wermeille, R. Felici, S. Ferrer, and J. W. M. Frenken, Nature Chemistry **2**, 730 (2010).

[13]J. Gustafson, M. Shipilin, C. Zhang, A. Stierle, U. Hejral, U. Ruett, O. Gutowski, P. A.

Carlsson, M. Skoglundh, and E. Lundgren, Science **343**, 758 (2014).

[14]I. K. Robinson and D. J. Tweet, Reports on Progress in Physics **55**, 599 (1992).

[15]G. Renaud, R. Lazzari, and F. Leroy, Surface Science Reports **64**, 255 (2009).

[16]T. Matsushima, T. Okuda, T. Eguchi, M. Ono, A. Harasawa, T. Wakita, A. Kataoka, M. Hamada, A. Kamoshida, Y. Hasegawa, and T. Kinoshita, Review of Scientific Instruments **75**, 2149 (2004).

[17]M. S. Rodrigues, O. Dhez, S. L. Denmat, J. Chevrier, R. Felici, and F. Comin, Journal of Instrumentation **3**, P12004 (2008).

[18]M. L. Cummings, T. Y. Chien, C. Preissner, V. Madhavan, D. Diesing, M. Bode, J. W. Freeland, and V. Rose, Ultramicroscopy **112**, 22 (2012).

[19]S. Rackwitz, I. Faus, B. Lägel, J. Linden, J. Marx, E. Oesterschulze, K. Schlage, H.-C. Wille, S. Wolff, A. J. Wolny, and V. Schünemann, Hyperfine Interactions **226**, 667 (2014).

[20]T. Slobodskyy, A. V. Zozulya, R. Tholapi, L. Liefeith, M. Fester, M. Sprung, and W. Hansen, Review of Scientific Instruments **86**, 065104 (2015).

[21]B. Gumí-Audenis, F. Carlà, M. V. Vitorino, A. Panzarella, L. Porcar, M. Boilot, S. Guerber, P. Bernard, M. S. Rodrigues, F. Sanz, M. I. Giannotti, and L. Costa, Journal of Synchrotron Radiation **22**, 1364 (2015).

[22]I. Schmid, J. Raabe, B. Sarafimov, C. Quitmann, S. Vranjkovic, Y. Pellmont, and H. Hug, Ultramicroscopy **110**, 1267 (2010).

[23]Z. Ren, F. Mastropietro, A. Davydok, S. Langlais, M.-I. Richard, J.-J. Furter, O. Thomas, M. Dupraz, M. Verdier, G. Beutier, P. Boesecke, and T. W. Cornelius, Journal of Synchrotron Radiation **21**, 1128 (2014).

[24]A. Saito, J. Maruyama, K. Manabe, K. Kitamoto, K. Takahashi, K. Takami, M. Yabashi, Y. Tanaka, D. Miwa, M. Ishii, Y. Takagi, M. Akai-Kasaya, S. Shin, T. Ishikawa, Y. Kuwahara, and M. Aono, Journal of Synchrotron Radiation **13**, 216 (2006).

[25]K. Tsuji, K. Wagatsuma, K. Sugiyama, K. Hiraga, and Y. Waseda, Surface and interface analysis **27**, 132 (1999).

[26]R. van Rijn, M. D. Ackermann, O. Balmes, T. Dufrane, A. Geluk, H. Gonzalez, H. Isern, E. de Kuyper, L. Petit, V. A. Sole, D. Wermeille, R. Felici, and J. W. M. Frenken, Review of Scientific Instruments **81**, 014101 (2010).

[27]O. Balmes, R. van Rijn, D. Wermeille, A. Resta, L. Petit, H. Isern, T. Dufrane, and R. Felici, Catalysis Today **145**, 220 (2009).

[28]M. J. Rost, L. Crama, P. Schakel, E. V. Tol, G. B. E. M. V. Velzen-Williams, C. F. Overgauw, H. T. Horst, H. Dekker, B. Okhuijsen, M. Seynen, A. Vijftigschild, P. Han, A. J. Katan, K. Schoots, R. Schumm, W. V. Loo, T. H. Oosterkamp, and J. W. M. Frenken, Review of Scientific Instruments **76**, 053710 (2005).

[29]R. van Rijn, O. Balmes, A. Resta, D. Wermeille, R. Westerstrom, J. Gustafson, R. Felici, E. Lundgren, and J. W. M. Frenken, Phys. Chem. Chem. Phys. **13**, 13167 (2011).

[30]W. G. Onderwaater, *CO oxidation catalysis at multiple length scales*, Ph.D. thesis, Leiden University (2016).

[31]B. L. M. Hendriksen and J. W. M. Frenken, Physical Review Letters **89**, 046101 (2002).

[32]S. B. Roobol, W. G. Onderwaater, J. Drnec, R. Felici, and J. W. M. Frenken, Journal of Applied Crystallography , 1 (2015).

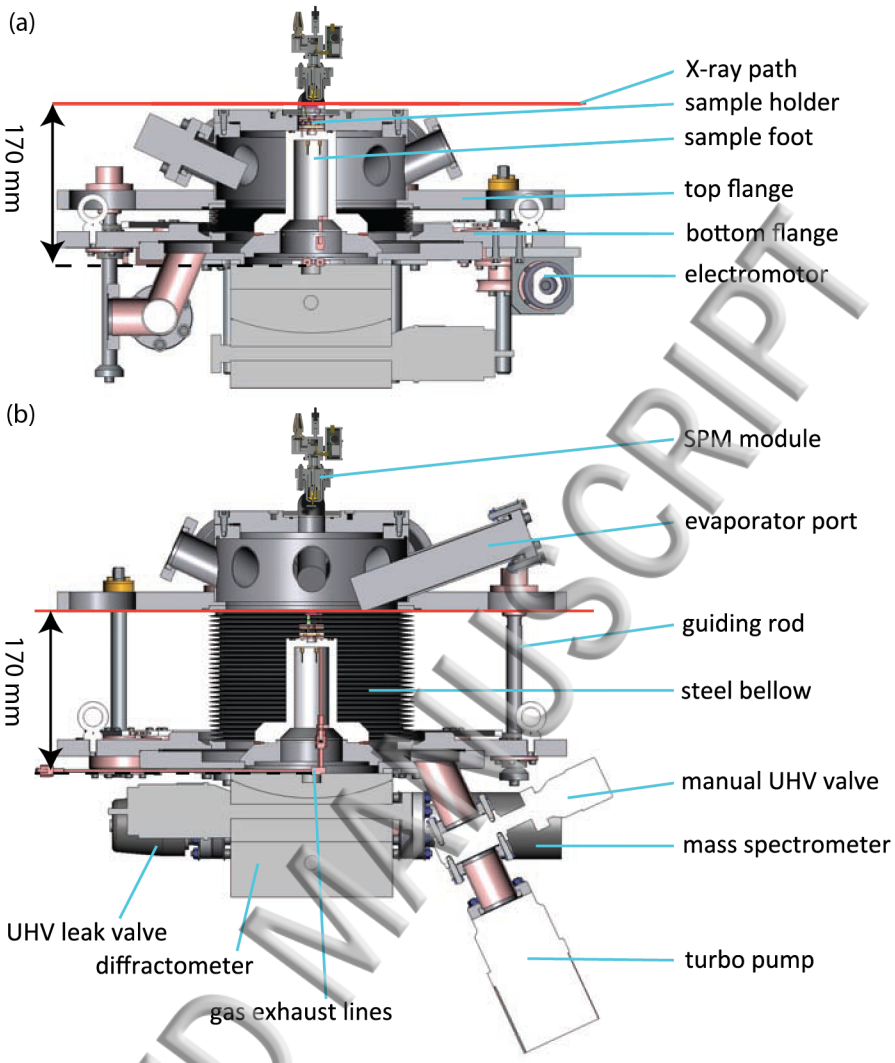

FIG. 1. Cross-sectional view of the complete SXRD + SPM system. The top flange of this chamber can be translated vertically. When the flange is at its lowest point, (a), the chamber is in measurement configuration. The sample is enclosed by the dome-shaped reactor, which is sealed off from the UHV part of the system. The X-ray beam now has a pathway to the sample. A quadrupole mass spectrometer is used to measure the composition of the gas that leaves the flow reactor via an exhaust capillary. When the flange is in the highest position, (b), the chamber is in the UHV preparation configuration. The SXRD system in Figure (b) is shown 90° rotated with respect to the view of Figure (a). The sample is exposed to UHV and is available for preparation purposes (ion bombardment, deposition, etc.). The SPM part is placed on top of the dome-shaped reactor, which is shown in more detail in Figure 2.

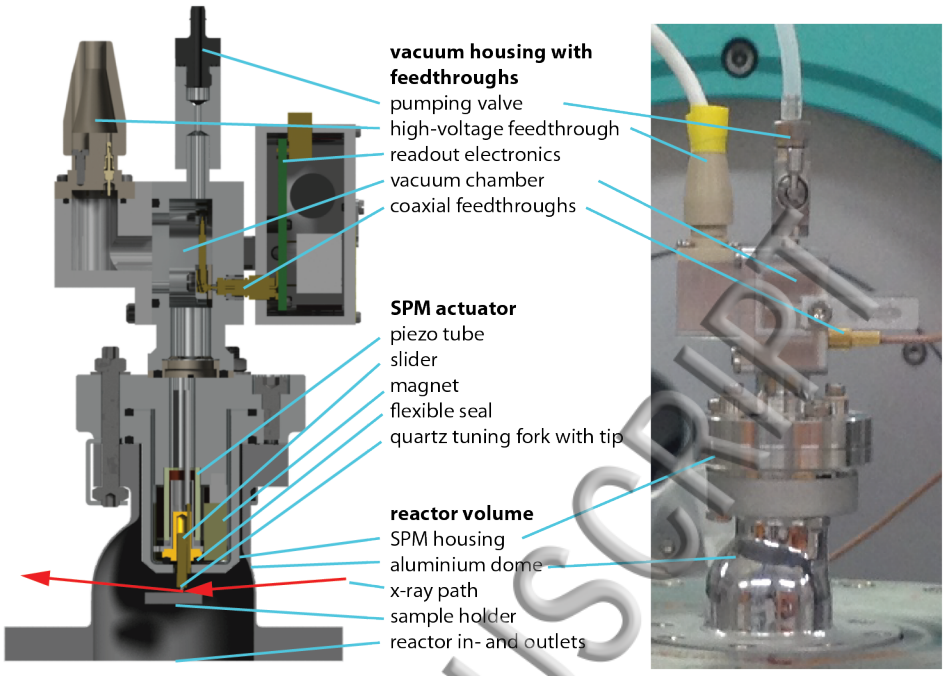

FIG. 2. Schematic cross section (left) and photograph (right) of the X-ray-transparent aluminum dome that defines the reactor volume. In the cross section, the sample is indicated together with incident and reflected X-rays (red arrows). The SPM part of the system is mounted on top of the dome and partially reaches into the dome. The STM tip or the AFM tuning fork with tip are located on the central axis of the dome and the sample. A flexible seal separates the high-pressure reactor volume from the vacuum that surrounds the piezo element. The cables at the top of the photograph connect the SPM unit to the control electronics, including a preamplifier that is positioned at 30 cm distance.

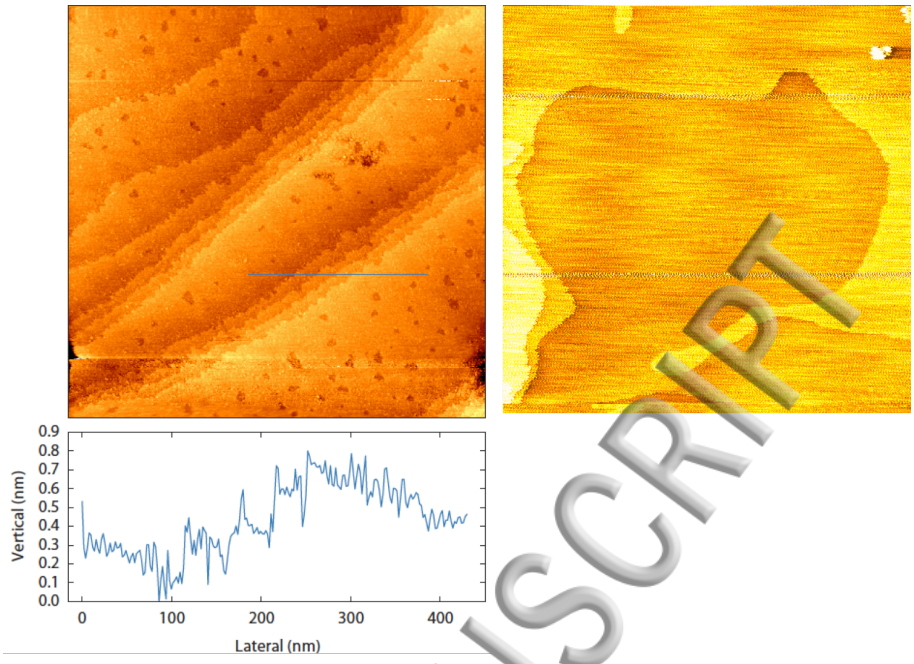

FIG. 3. Left panel: Au(111) surface scanned by the SPM setup in STM mode. For these measurements, the SPM was mounted on a table-top catalysis chamber very similar to the ReactorSXRD chamber and this was placed on a vibration isolation stage. Individual atomic steps are well resolved in the images measured under these conditions. The Au(111) surface is partially covered with traces of sulfur, resulting in the monolayer-deep holes in the surface. Right panel: similar STM image obtained on another Au(111) surface, with the ReactorSXRD mounted on the diffractometer of beamline ID03 at the ESRF. The lower left panel shows a characteristic height profile, obtained along the line segment indicated in the STM image. Note that in both images, the atomic steps on the Au surface can be distinguished. The images have dimensions of 1000 $\times$ 1000 nm^2 and 640 $\times$ 640 nm^2, respectively and were taken with sample bias voltages of 0.5 and -1.0 V and tunneling currents of 0.05 and 1.4 nA, respectively.

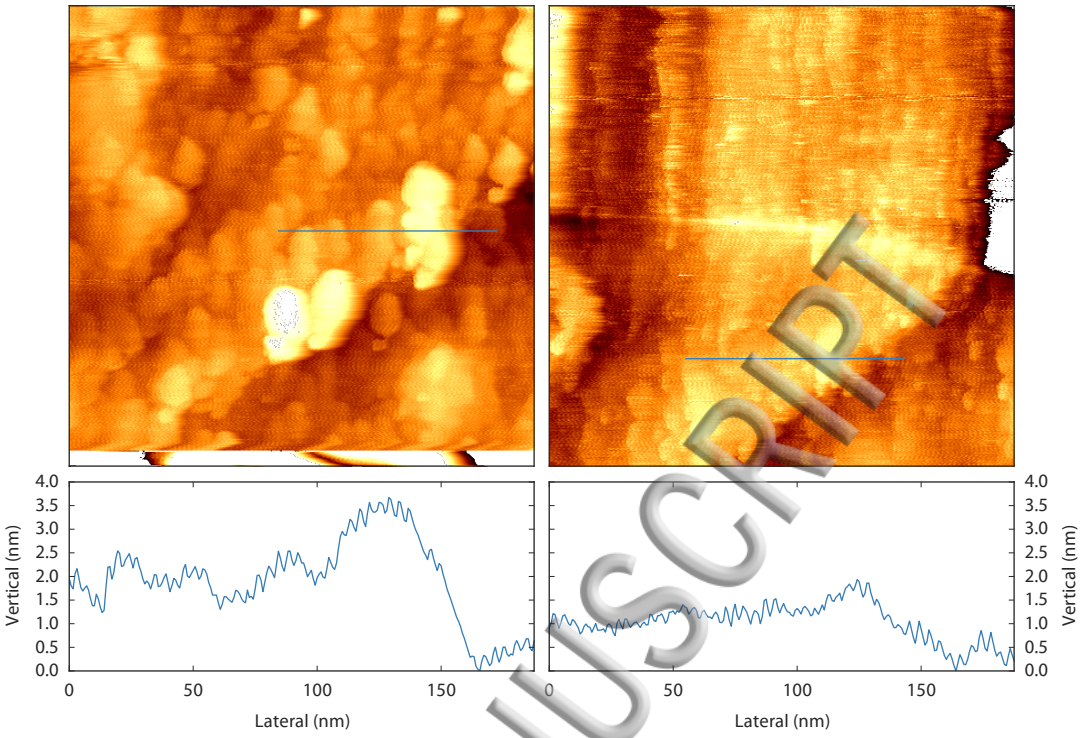

FIG. 4. Pd(100) surface scanned by the SPM setup in STM mode. The two images show the surface in a mixture of CO and O_2 at 1.1 bar and 300 °C. The left-hand image is measured in a flow of 3 ml/min CO and 55 ml/min O_2. The right-hand image shows the same region, after changing the gas mixture in the reactor to a flow of 20 ml/min CO and 38 ml/min O_2. The surface has transformed radically after changing the gas mixture which we ascribe to a reduction of the oxide on the surface. The height profiles in the two lower panels show more or less the same region on the surface. The height variations in the right panel have been reduced by roughly a factor two with respect to those in the left panel. Both images have dimensions of 400 × 400 nm^2 and were taken with a sample bias voltage of -0.2 V and a tunneling current of 0.1 nA in acquisition times of 105 s.

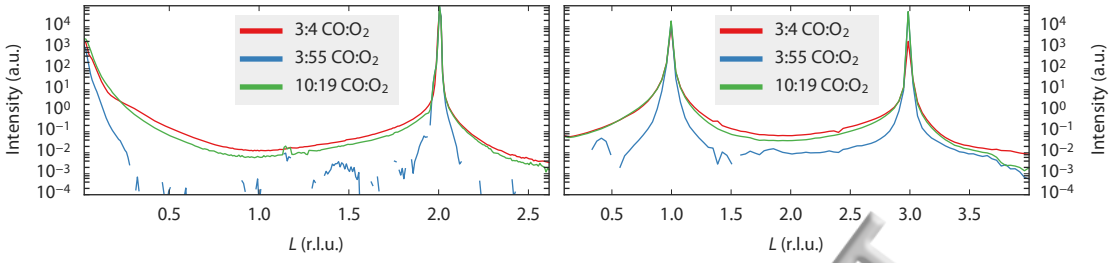

FIG. 5. X-ray reflectivity curve (left) and [1 0 l] crystal truncation rod (right) of Pd(100) during exposure to three different O_2 and CO mixtures at a temperature of 300 °C and at a pressure of 1.1 bar. The reciprocal lattice units (*r.l.u.*) are based on the surface unit cell of the Pd(100) surface with two axes parallel to the surface ($|\vec{a}_1| = |\vec{a}_2| = a_0/\sqrt{2}$) and one perpendicular to the surface ($|\vec{a}_3| = a_0$) where $a_0 = 3.89$ $\mathring{A}$. The intensity of the reflectivity curve decreases very fast from low L values upwards in the oxidized regime (blue curve) indicating increased surface roughness. A small shoulder in the crystal truncation rod resulting from diffraction of the oxide is visible at 0.4 *r.l.u.* confirming that the sample is oxidized in the a flow of 3 ml/min CO and 55 ml/min O_2. After switching to a flow of 20 ml/min CO and 38 ml/min O_2 this peak disappears and the intensities measured in the initial flow of 30 ml/min CO and 40 ml/min O_2 are almost fully recovered for both the reflectivity curve and crystal truncation rod, indicating that the surface has smoothened considerably upon reduction.

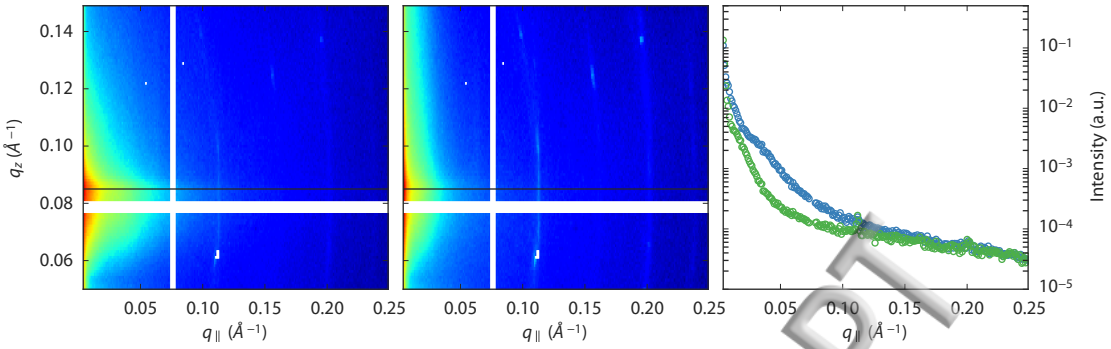

FIG. 6. Two GISAXS patterns of the Pd(100) surface at a temperature of 300 °C and at a pressure of 1.1 bar in a gas mixture of O_2 and CO. The images are measured in a flow of 3 ml/min CO and 55 ml/min O_2 in the left-hand panel and a flow of 20 ml/min CO and 38 ml/min O_2 in the center panel. The GISAXS images have been processed with the BINoculars software[32]. The white horizontal and vertical bands are inactive areas in the Maxipix detector. The panel on the right shows cuts through both patterns at the location of the Yoneda peak at $q_z = 0.085$ Å^{-1} (indicated in the two images by the horizontal black lines) for a flow of 3 ml/min CO and 55 ml/min O_2 (blue symbols) and for a flow of 20 ml/min CO and 38 ml/min O_2 (green symbols). The rings visible at $q_\parallel = 0.1$ Å^{-1} and 0.2 Å^{-1} result from scattering of the reflected X-ray beam from the aluminum window.